Flexible and Printed Electronics

PAPER • OPEN ACCESS

Inkjet-printed transistors with coffee ring aligned carbon nanotubes

To cite this article: Paria Naderi and Gerd Grau 2024 *Flex. Print. Electron.* **9** 015001

IOP Publishing Flex. Print. Electron. 9 (2024) 015001 https://doi.org/10.1088/2058-8585/ad1ccf

Flexible and Printed Electronics

OPEN ACCESS

RECEIVED
13 June 2023

REVISED
22 December 2023

ACCEPTED FOR PUBLICATION
9 January 2024

PUBLISHED
19 January 2024

PAPER

Inkjet-printed transistors with coffee ring aligned carbon nanotubes

Paria Naderi* and **Gerd Grau**

Department of Electrical Engineering and Computer Science, York University, Toronto, Canada
* Author to whom any correspondence should be addressed.

E-mail: panaderi@yorku.ca

Keywords: thin-film transistors (TFTs), inkjet printing, carbon nanotubes (CNTs), coffee ring effect, solution processing, printed electronics

Supplementary material for this article is available online

Abstract

Low-concentration deposition techniques such as inkjet printing for forming carbon nanotube (CNT) transistor channels typically result in higher on–off current ratio, while lowering the field-effect mobility compared to traditional high-concentration techniques. In this paper, we show that inkjet-printed devices can have both high field-effect mobility and on–off current ratio by utilizing coffee ring induced thickness variation in the channel. The coffee ring effect occurs naturally in printed patterns with most solvents and substrates, and it pushes dissolved particles to the edges of printed features. Thickness variation and coffee ring effect are usually avoided in the channel of solution processed thin-film transistors by implementing additional expensive steps in the fabrication process. Instead, here, we control these variations and utilize them to create inkjet-printed CNT channels with printing induced thickness variation that improves transistor properties. Printing properties such as printing speed, and number of layers are studied to manipulate capillary flow and form thicker line edges, which ultimately enhance current transport in the CNT network. A two-pass printing pattern with separate lines improves the field-effect mobility five times compared to a pattern with connected lines that has no defined edges. The field-effect mobility increases from 1.1 to 5.7 cm^2 V^{-1} s^{-1} at a drain voltage of −2 V.

1. Introduction

An important research focus in the area of printed thin-film transistors (TFTs) is to explore simple, inexpensive and versatile fabrication processes for large-area electronics. For instance, conventional TFTs used in active-matrix backplanes are rigid and their fabrication needs chemicals for etching, masks, and expensive vacuum processes. Printing is a solution processing approach to realize low-cost and low-temperature electronics on a variety of substrates [1–3]. Direct-write printing techniques such as inkjet and aerosol jet are advantageous for rapid prototyping and the ability to modify the design while printing [4]. Moreover, inkjet printing can cover a larger range of film thickness and pattern width, and has high edge sharpness compared to other printing techniques [5]. It is widely considered as a promising technique to deposit carbon nanotube (CNT) inks for the channel of TFTs [6, 7]. CNT TFTs are used in flexible displays and electronic circuits, mainly as switches and invertors [8–10]. As-grown CNTs have a large number of metallic tubes, whereas CNT inks with high semiconducting percentage have been successfully formulated [11, 12]. CNT inks have been deposited as thin films using inkjet printing to make TFTs [7, 10, 13, 14], strain and chemical sensors [15, 16], and conductive films [17, 18]. When choosing the proper deposition technique for CNTs in TFT channels, one usually needs to compromise between high mobility and high on–off current ratio. High-density solution processing techniques such as drop casting [19] and spin-coating [20] lead to high field-effect mobilities and low on–off current ratio, while low-density techniques such as spray-coating [8, 19] and inkjet printing [21, 22], in general, lead to higher on–off current ratio at the cost of lowering the field-effect mobility. Additionally, it is difficult to maintain both high transistor current and low leakage current with any deposition technique [23].

Generally, film thickness non-uniformity is avoided when a layer is solution-processed for a device [24, 25]. The coffee ring effect is a major challenge when forming films from solutions. The coffee ring is the ring-shaped pattern that is left around the edge of printed patterns after the solvent evaporates. During the evaporation process, the edge of the droplet evaporates faster. The contact line, which is the interface of the solid, liquid and the surrounding vapor, is pinned. The contact line tends to stay pinned, therefore, the loss of solvent is compensated by liquid flowing from center to the edges. As a result, this capillary flow takes most of the solute to the edges [26]. In the case of lines, the pattern will be linear instead of circular. Researchers have been working on removing the coffee ring effect in CNT TFTs, since it causes the aggregation of the tubes on the edges of the printed pattern [27, 28]. One way to eliminate it is by eliminating the pinning, for instance by using a non-wetting substrate [29], or reversing the capillary flow by using a mixed solvent system [30–32]. At the same time, careful control over squeezing CNTs at desirable locations can help regulate their position and film morphology in the TFT channel. The performance of CNT TFTs improves by regulating CNTs inside the TFT channel using solution processing techniques [23, 33, 34]. With inkjet printing, CNTs can be aligned on droplet edges as a result of capillary flow [17, 35]. Tilted drop-casting causes the CNTs to exhibit liquid crystal behavior in the vicinity of the receding contact line, which causes regulated bundles of CNTs to form due to the high local concentration of CNTs [33]. Modulating the density of CNTs by inkjet printing fewer number of layers in the channel region closer to the source and drain electrodes lowers the energy barrier for injection of electrons [23]. As coffee ring effect naturally occurs as the film is forming, utilizing it rather than trying to prevent it will obviate the requirement for surface treatment [27] or the use of multiple solvents to reverse capillary flow [35]. Therefore, it is more convenient and agrees well with the nature of inexpensive solution processed printed electronics to engineer and utilize this effect.

From a fundamental perspective, four parameters influence the formation of coffee ring effect: ink concentration, substrate surface roughness, printing stage temperature, and stage speed or droplet deposition rate.

As the droplet evaporates, variations in solvent evaporation rate within the droplet induce convective currents, impacting the distribution of the solutes, within the droplet [36]. Increasing solute concentration causes an increase in the particle concentration in the coffee ring edge, since the increase in the solute concentration enhances the pinning of the contact line. However, the final coffee ring intensity depends on both capillary and Marangoni flows which are in opposite directions. In the case of many CNT inks, due to the presence of surfactants, increasing the concentration results in a negative surface tension gradient toward the droplet edge and thus an inward Marangoni flow [37, 38]. As a result, there is an optimal CNT ink concentration, which can lead to the maximum coffee ring effect.

In addition to pinning due to accelerated drying at the edges, surface roughness of the substrate can also cause pinning of the contact line. According to the Wenzel model, $\cos\theta^* = r\cos\theta$, where θ^* is the apparent contact angle, r is the roughness of the smooth surface, and θ is the intrinsic contact angle of the ideal smooth surface. Increasing roughness (r), decreases the apparent contact angle (θ^*) [39], which means stronger pinning of the contact line, and thus a stronger coffee ring effect.

The flow dynamics of the particles inside a printed droplet or line is the result of non-uniform evaporation flux along the droplet interface and potentially a temperature gradient in the droplet [40–43]. The outward capillary flow that moves the solute particles to the edge of the droplet is evaporation-driven, meaning that by increasing substrate temperature the transfer of solute increases, which ultimately increases the coffee ring effect. However, the final coffee ring patterns are a product of both capillary and Marangoni flows. On a heated substrate the droplet surface closer to the edge is warmer than the apex, therefore it has lower surface tension. This causes a circular Marangoni flow from the droplet apex to the edge on the surface and toward the droplet center in the bulk.

Droplet deposition rate controls the time between successive droplets during which the ink can flow to the edges of the line, can flow between adjacent droplets, and dry. Decreasing the stage speed means decreasing droplet deposition rate, which leads to a longer time between droplets relative to the drying time analogous to higher stage temperature at a higher stage speed. This effect can be exploited to print lines on challenging substrates using the stacked-coin morphology [43]. Here, the effect of deposition rate on coffee ring effect in lines is studied.

Here, we present CNT TFTs with an inkjet-printed CNT channel. With drop-on-demand inkjet printing, lines with controlled morphologies were printed on an Si/SiO_2 wafer. Inkjet printing parameters were varied to manipulate the formation of the coffee ring effect in the channel of the TFTs. When separate lines were printed, due to the coffee ring effect, thicker edges were formed while connected lines dried uniformly with random puddles formed in the pattern. Transistor I–V characteristics and contact resistance at the CNT/metal interfaces were studied. Thickness profiles and atomic force microscopy (AFM) images of the printed CNT channels show tube configurations in the CNT networks that explain the device behavior.

2. Experimental section

2.1. Substrate preparation

P-type silicon wafers with a 300 nm oxide layer (University Wafers, Inc., South Boston, USA) were used as substrates with the p^{++} silicon as the gate electrode. The silicon wafers were cut and sonicated in isopropanol, acetone, and deionized (DI) water each for 10 min. Next, they were dried with air and were plasma treated at 50 W for 1 min. Prior to CNT printing, the surface was functionalized by drop-casting poly-L-lysine (PLL, 0.1% w/v in water, Sigma Aldrich, Canada) for 5 min, followed by rinsing with DI water, drying with air, and storing in a desiccator for 20 min. PLL is commonly used to increase the adhesion of solution processed carbon nanotubes to the surface of silicon dioxide (SiO_2) [4, 44, 45]. PLL is a biocompatible polymer with a positive charge which forms a stable layer by adsorbing to the negatively charged SiO_2 present on the surface.

2.2. Inkjet printing CNT channel

The CNT solution with a 1 mg ml^{-1} concentration and 99.9% semiconducting tubes (IsoNanotubes-S, NanoIntegris Technologies, Inc., Quebec, Canada) was used as purchased without further dilution. A custom-built inkjet printer with a 60 μm diameter nozzle (Microfab Technologies, Inc., Plano, TX) was used. A pulse with a voltage of 23 V, rise and fall time of 12 μs, and dwell and echo time of 40 μs was used to jet the droplets. The printed patterns were stored in a desiccator for 24 h. Next, they were rinsed with DI water, dried and finally annealed at 100 °C for 30 min. In the case of two-pass prints, after this step, a second pass was printed with lines offset by half the line spacing to ensure the coffee ring was located between the coffee ring lines of the first pass printed lines, followed by rinsing and annealing in the same way. As a control, the CNT solution was also drop-cast on the as-cleaned and functionalized silicon substrates for 2 h. Then, they were rinsed also, dried and annealed at 100 °C for 30 min.

2.3. Inkjet printing CNT line patterns

Parallel lines of the CNT solution were inkjet-printed in the channel of a TFT with a bottom-gate-top-contact device configuration. The reason for adopting a top-contact configuration was that to print the CNT lines and engineer the coffee ring effect in the printed lines, it was necessary to have a flat surface on which the capillary flow has its natural direction toward the edges of the pattern. While in a bottom-contact configuration, the silver electrodes add thickness, roughness, and surface energy variation to the surface, which would disrupt the formation of the CNT coffee ring patterns.

During the printing process, the line spacing, number of layers, and the stage speed were varied for each experiment, while the drop spacing was kept constant (90 μm) for all the experiments. The line spacing changes the overall concentration of CNTs inside the channel and it was kept constant for a given number of layers. Figure 1 shows the device fabrication process in the following steps: functionalization of the SiO_2 surface with PLL, printing CNT ink in three different patterns (one-pass connected, one-pass separate, and two-pass separate lines), rinsing and annealing of the ink solvent and additives, and printing source and drain electrodes with silver nanoparticle ink. In one-pass connected lines, there is no separation between the lines and no defined coffee ring is formed across the lines, instead a layer with non-uniform thickness forms (figure 1, first row). In the one-pass separate lines pattern, lines are printed with a line spacing between them (figure 1, second row). This spacing was chosen to be the minimum before the lines would merge. The coffee ring effect can be seen in the thickness profiles of printed CNT solution in separate lines (figure 1, second row, inset figure). To achieve two-pass separate lines, after the one-pass separate lines were rinsed and annealed, a second pass of lines was printed with an offset of half the line spacing, followed by rinsing and annealing of the patterns (figure 1, third row). After rinsing and annealing of the ink, the CNTs remain on the surface. The channel length and width of the devices are 80 μm and 1300 μm, respectively.

The CNT concentration for one-pass connected and two-pass separate lines is 4.2×10^{-5} mg cm^{-2} after printing before rinsing, while the one-pass separate lines pattern has half the concentration. The following formula was used to calculate CNT concentration per cm^2 printed in the transistor channel:

$$\frac{\text{Droplet volume (ml)} \times \text{CNT percentage in the solution} \left(\frac{\text{mg}}{\text{ml}}\right) \times \text{number of layers}}{\text{Drop spacing (cm)} \times \text{line spacing (cm)}}.$$

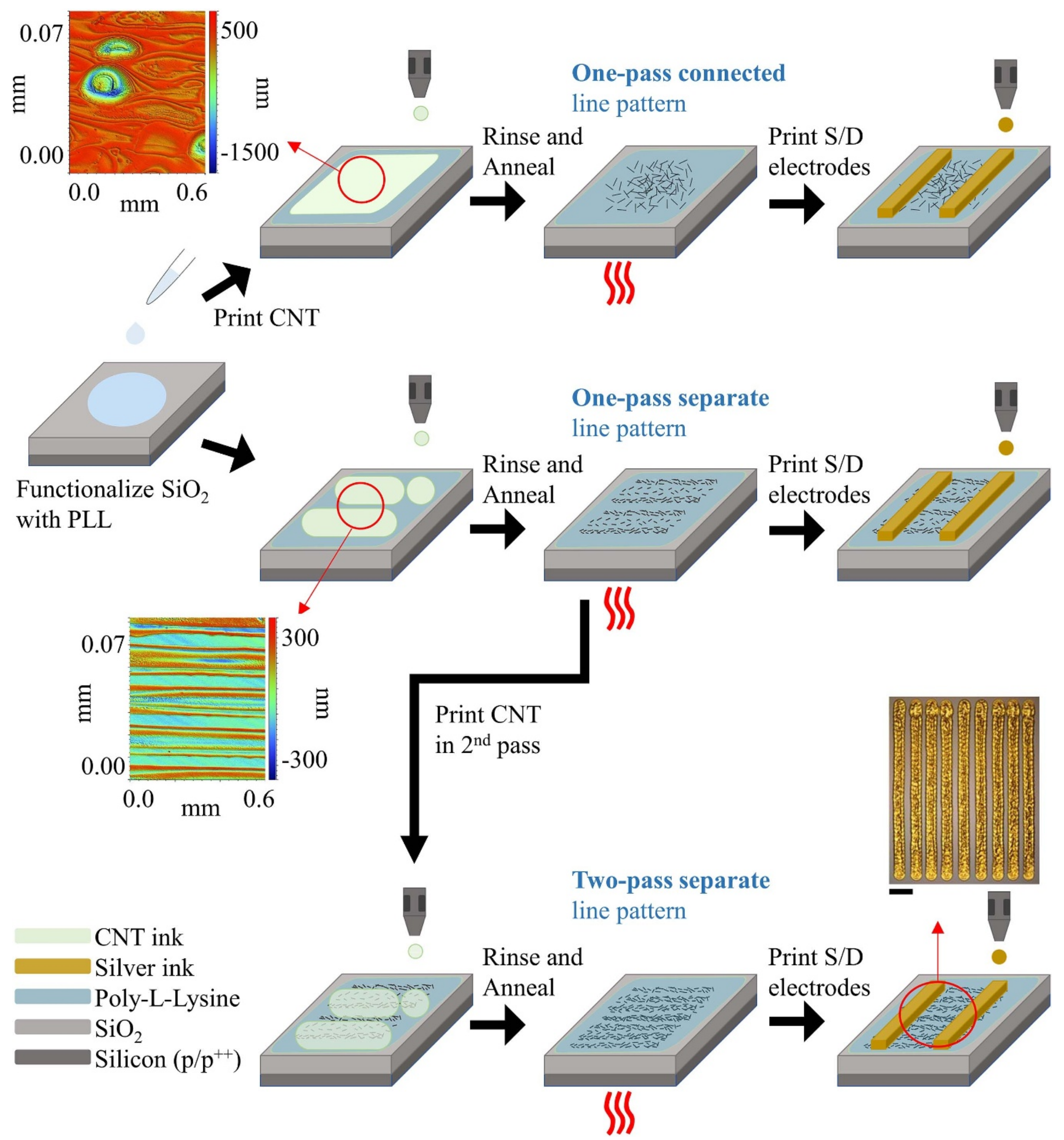

Figure 1. The transistor fabrication process in the following steps: functionalization of the SiO_2 surface with poly-L-lysine, printing CNT ink in three different patterns (one-pass connected, one-pass separate, and two-pass separate lines), rinsing and annealing of the ink solvent and additives, and printing source and drain electrodes with silver nanoparticle ink. In one-pass connected lines, there is no separation between the lines and no defined coffee ring is formed across the lines. In two-pass separate lines, after the one-pass separate lines are rinsed and annealed, a second pass of lines are printed with an offset of half the line spacing. Inset figures: thickness profiles of printed CNT solution in connected lines (first row) and in separate lines (second row), and optical micrograph of TFTs with channel lengths of 60 and 80 μm (third row) where the scale bar represents 200 μm.

Where in the case of two-pass printed lines, the droplet volume, the CNT percentage in the solution, the number of layers, drop spacing, and line spacing are 1.13×10^{-7} ml, 0.01 mg ml^{-1}, 3, 90 μm and 180 μm, respectively. With the pattern printed twice, CNT concentration becomes 4.2×10^{-5} mg cm^{-2}. In the case of a one-pass connected line pattern, the line spacing is half (90 μm), therefore resulting in the same value.

Despite the ink concentration being held constant to achieve stable jetting, the variation in the number of printed layers led to changes in CNT concentration per unit area within the lines. To ensure a uniform monolayer for good adhesion between the CNTs and the substrate and thus uniform surface roughness, the PLL-functionalized SiO_2 surface underwent thorough rinsing and was stored in a desiccator, following the same procedure for all samples. The temperature of the printing stage remained constant between experiments to remove it as a confounding factor that would affect both coffee ring effect and annealing of the CNT film. In our experiments, the stage speed, i.e. droplet deposition rate, was deliberately varied to control the coffee ring effect.

2.4. Inkjet printing source and drain electrodes

Source and drain electrodes were inkjet-printed on top of the CNT layer on a heated stage (stacked-coin [43]) at 120 °C using silver nanoparticle ink (ANP DGP 40LT-15C, Advanced Nano Products, Co., Sejong, Korea) with a 60 μm diameter nozzle (Microfab Technologies, Inc., Plano, TX). The silver nanoparticle source and drain electrodes were printed with a length of 2 mm (figure 1, third row, inset figure) while the width of the printed channels is 1300 μm in order to minimize leakage currents.

Heating the stage is necessary to stop the silver ink from spreading nonuniformly on the previously deposited CNT network. The stage temperature at the time of printing the electrodes is 120 °C which is not much higher than the CNT annealing temperature (100 °C). In fact, it has been shown that CNT exposure to high temperature further removes the solvent and surfactant causing a resistance barrier reduction in the CNT network which leads to higher conductivity and transparency [46]. Not to mention that thermal annealing of CNT layers can also increase their mechanical stability [47]. Therefore, it is assumed that the heated stage leads to further solvent removal and increasing conductivity of the CNT channel.

2.5. Characterization

The transistor I–V characteristics were obtained using a semiconductor parameter analyzer (Keithley 4200, Tektronix). AFM images were taken with a Multimode 8-HR scanning probe microscope (Bruker, Germany). The imaging mode was ScanAssist-air. Thickness profiles were taken with a Contour CT-K optical profiler (Bruker Nano, Inc., Arizona, USA). The error bars and the average values were calculated over 8–11 devices for each printed pattern.

3. Results and discussion

Two factors, number of layers and printing speed, which controls delay between adjacent droplets, were used to adjust the intensity of the coffee ring effect. Figure 2(a) shows 2D optical thickness profiles of CNT lines printed without separation (connected lines). One-pass connected lines result in a random distribution of the CNT solution on the substrate with the formation of occasional puddles. Figure 2(b) shows separate lines printed with low speed (100 μm s^{-1}). At low speed, due to the longer delay in printing between subsequent droplets, droplets are dried and pinned before the next droplet hits the substrate while the intersection of the two adjacent droplets redissolves as the second drop is printed. In contrast, at higher speed, each incoming droplet promptly merges with its predecessor, resulting in a larger liquid ink amount, an increased capillary flow toward the pattern edges, and a stronger coffee ring effect. The addition of layers to the pattern serves to amplify the coffee ring effect in the same manner. Figure 2(c) shows separate lines printed with one, two, three and four layers of CNT solution from left to right, respectively, all printed with a speed of 400 μm s^{-1}. Figure 2(d) shows the corresponding 1D thickness profiles across the printed lines in the y-direction for the different number of layers. The thickness variation across each line in figures 2(c) and (d) is negligible for one layer, while for three and four layers, there is larger thickness at the edges compared to the center of the lines, i.e. a coffee ring was formed. AFM images of the lines in figures 2(c) and (d) are presented in supplementary information (figure SI 5). All the thickness profiles were taken before rinsing and annealing of the patterns, with fillers, binders, and additives of the ink still present, which makes it challenging to observe individual nanotubes in the AFM images but optical profilometry and AFM show the same trends. In the fabrication process of two-pass separate lines patterns, the acquisition of a thickness profile, which is amplified by the presence of the fillers, binders, and additives of the ink, to demonstrate the two-pass profile is not possible since the first pass of printed CNTs is rinsed before printing the second pass. Figure 2(e) shows plots of two transistor metrics, the on–off current ratio and the field-effect mobility versus the number of layers for transistors printed at 400 μm s^{-1}. In all the plots, the metrics were extracted from linear transfer characteristics ($I_d V_g$) of devices measured at $V_d = -5$ V. Increasing the number of layers improves the device performance up to a certain point and after that point (from four layers) the performance deteriorates. This can be explained by the optical thickness profile of printed lines with four layers in figures 2(c) and (d). For a larger number of layers, thicker line edges are formed, however the center of the lines are not depleted of material as it is the case in lines with three layers. This means that enhanced performance is due to the coffee ring effect and not simply the overall CNT concentration in the channel. Figure 2(f) shows plots of the same device properties versus printing speed for transistors printed with three layers. Increasing printing speed enhances the coffee ring effect and this improves device properties. However, the direct speed–performance relationship breaks down at high speed. The reason is that at higher printing speed, while material is pushed to the line edges, it is also pushed to the ends of the lines, ultimately reducing the CNT concentration in the channel (see supplementary information, figure SI 2).

After exploring the factors affecting the coffee ring effect, transistors with the most pronounced line edges (printed with three layers and at 400 μm s^{-1}) were compared with a connected pattern without a gap between the lines. Such a connected pattern is conventionally used in printed CNT TFTs and does

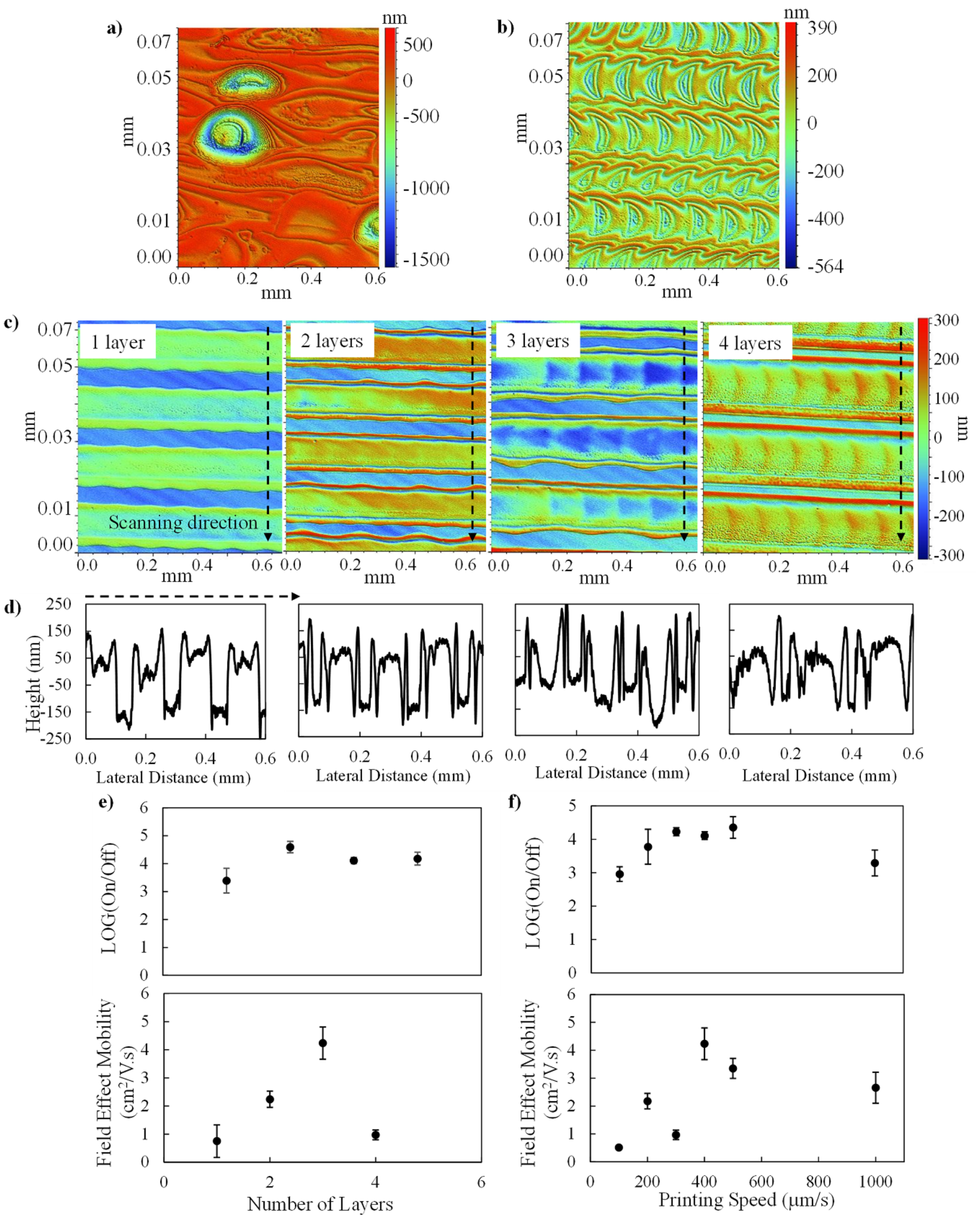

Figure 2. 2D optical thickness profiles of (a) lines printed without separation (connected lines), (b) separate lines printed at low speed (100 μm s^{-1}), and (c) separate lines with one, two, three, and four layers from left to right printed with a speed of 400 μm s^{-1}. (d) The corresponding 1D thickness profiles across the lines for lines in (c). Dashed lines in (c) show the scanning direction where the x–z coordinates were extracted from the 2D optical profile images. The coffee ring effect is most intense in films with three layers. Log of on–off current ratio and field-effect mobility measured at $V_d = -5$ V (e) versus number of printed lines at 400 μm s^{-1}, and (f) versus printing speed for printed lines with three layers.

not exhibit clearly defined coffee ring lines in the channel [7, 13, 44, 48].

Figures 3(a) and (b) show the transfer characteristics for two-pass separate, one-pass separate, and one-pass connected line patterns measured at $V_d = -2$ V on logarithmic and linear scales, respectively. From one-pass connected and one-pass separate and to two-pass separate line patterns, a shift of threshold voltage (V_t) toward negative gate voltage is observed, and V_t changes from 11.4 V to 12 V to 8.4 V. The separate-line patterns result in devices with better performance. From one-pass connected to one-pass separate to two-pass separate lines, the field-effect mobility increases from 1.1 to 1.5 to 5.7 cm^2 V^{-1} s^{-1} and the on–off current ratio changes from 2.3×10^5 to 8.2×10^5 to 3.6×10^5 at $V_d = -2$ V. These performance metrics are summarized in table 1. One-pass separate lines have the highest on–off current

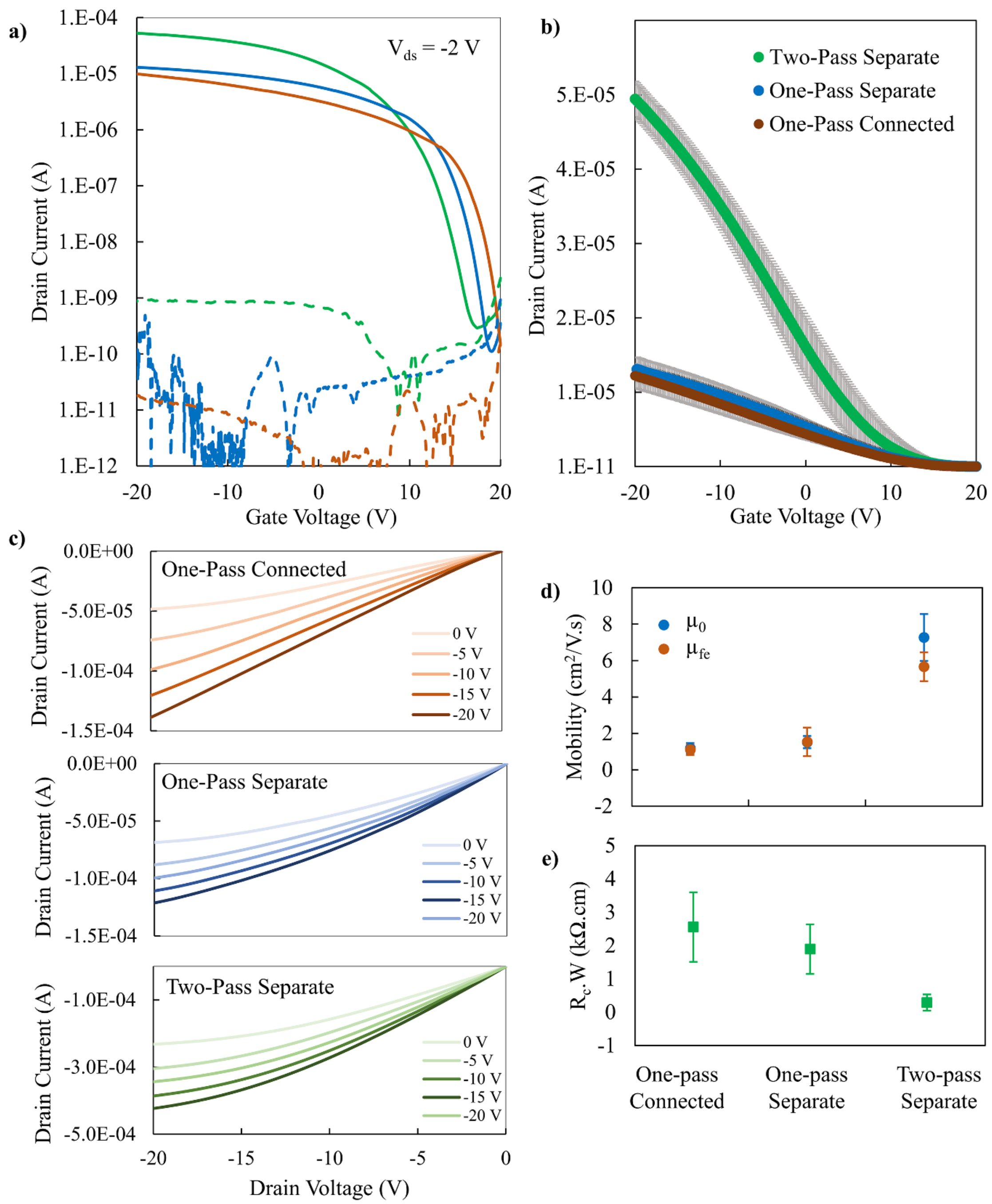

Figure 3. (a) Transfer characteristics of the three printing patterns at $V_{ds} = -2$ V on a log scale. Dashed curves are gate current for each printing pattern and colors are the same as in (b). (b) The same transfer characteristics on a linear scale with error bars representing 8–11 devices. (c) Output characteristics of a representative transistor for each pattern, from top to bottom: one-pass connected, one-pass separate and two-pass separate lines. (d) Field-effect (μ_{fe}) and low-field (μ_0) mobilities and (e) width normalized contact resistance (R_cW) for the three patterns. The two-pass separate line pattern improves the devices in two ways: increasing the low-field mobility of the carriers in the channel and decreasing the contact resistance.

ratio due to lower concentration of CNTs. With this coffee ring methodology, with equal overall concentrations of CNTs (from one-pass connected to two-pass separate), the device properties improve remarkably. However, the off-current and the gate leakage current increase slightly as well although the CNT concentration remains unchanged from one-pass connected to two-pass separate lines. Figure 3(c) shows the output characteristics ($I_d V_d$) of one-pass connected, one-pass separate and two-pass separate line patterns from top to bottom, respectively. The curvature in $I_d V_d$ characteristics at low V_d in the one-pass connected line pattern is an indication of a non-ohmic contact [49], while the drain current does not saturate at high V_d. Conversely, in devices with two-pass separate line patterns, the linear regime has a constant slope, and the drain current almost saturates at high V_d. Devices with one-pass separate line pattern also exhibit improved behavior compared to one-pass connected lines.

Table 1. Transistor performance metrics for different CNT deposition patterns in the channel.

Pattern	μ_{fe} ($cm^2\ V^{-1}\ s^{-1}$)	I_{on} (A)	V_t (V)
One-pass connected	1.1	1.2×10^{-5}	11.4
One-pass separate	1.5	1.6×10^{-5}	12
Two-pass separate	5.7	4.9×10^{-5}	8.4

Two-pass separate lines pattern has an equal concentration of CNTs compared to one-pass connected pattern. However, it demonstrates higher field-effect mobility and current transporting capacity. To investigate the device behavior further, we studied the channel and the contacts by calculating low-field mobility and contact resistance. Using the Y-function method (YFM), the width normalized contact resistance and the low-field mobility of the three printing patterns (two-pass separate, one-pass separate and one-pass connected) were extracted. Low-field mobility is the intrinsic carrier mobility (μ_0) and field-effect mobility (μ_{fe}) is the carrier mobility in the presence of an electric field which is influenced by contact effects. The Y-function is defined as:

$$Y = \frac{I_d}{\sqrt{g_m}} = \sqrt{\frac{W}{L} C_{ox} \mu_0 V_d} \times \left(V_g - V_t\right) \quad (1)$$

where g_m, W, L, C_{ox}, and μ_0 are transconductance, transistor width and length, dielectric capacitance per unit area (here SiO_2), and low-field mobility, respectively. Using the transfer characteristics in the linear regime ($V_d = -2$ V) and from the slope and the y-intercept of Y versus V_g, μ_0 and V_t are extracted [50, 51]. Later, using equation (2), and by extracting the x-intercept of $\frac{1}{\sqrt{g_m}}$ versus $V_g - V_t$, θ is extracted

$$\frac{1}{\sqrt{g_m}} = \frac{1 + \theta\left(V_g - V_t\right)}{\sqrt{\frac{W}{L} C_{ox} \mu_0 V_d}} \quad (2)$$

and,

$$\theta = \theta_0 + \theta^* = \theta_0 + G_m \times R_{sd} \quad (3)$$

where $\theta_0 \left(\approx 0\right)$, G_m and R_{sd} are the mobility reduction coefficient, the transconductance parameter and the total source and drain resistances which in the case of identical electrodes is defined as:

$$R_{sd} = 2 \times R_c \quad (4)$$

where R_c is the contact resistance associated with one electrode. The Y-function allows the extraction of contact resistance from individual devices. The results in figures 3(d) and (e) show a remarkable increase of both field-effect (derived from the transfer characteristics) and low-field mobilities and the decrease of contact resistance in the two-pass separate lines pattern compared to the other patterns. The low-field mobility increases from 1.2 to 1.5 to 7.3 $cm^2\ V^{-1}\ s^{-1}$ while the width normalized contact resistance changes from 2.6 to 1.9 to 0.3 kΩ·cm for one-pass connected, one-pass separate and two-pass separate lines, respectively.

For the purpose of comparison, devices with drop-cast CNTs were also fabricated and characterized. Inkjet printing is an efficient way of increasing on–off current ratio compared to non-patterned solution deposition techniques such as drop-casting. However, it has been reported that the mobility usually decreases due to the decrease in the CNT concentration. Here, both criteria have been achieved. Non-patterned drop-cast devices exhibit a mobility of 7.5 $cm^2\ V^{-1}\ s^{-1}$, and an on–off current ratio of 8.2×10^2, at $V_d = -5$ V, while for two-pass separate line patterns, these figures are 5.7 $cm^2\ V^{-1}\ s^{-1}$ and 3.6×10^5, respectively. Not to mention that for unpatterned drop-cast devices, the maximum gate leakage current is 7.6×10^{-5} A as opposed to the much lower gate leakage current of 2.18×10^{-10} A achieved with printed two-pass separate lines.

To investigate the device behavior microscopically, AFM images of the channels of four printed patterns were taken. The thickness profiles previously shown in figure 2 represent the printed CNT channels before rinsing off the additives in the ink. The un-rinsed profiles show the solute distribution across the printed lines. After rinsing and annealing of the samples, the CNTs remain on the surface as shown in figure 4 with a thickness of a few nanometers as the surface functionalization with PLL ensures the adhesion of a thin layer of tubes to the surface [52]. Figure 4(a) shows the randomness of the tubes in the channel in a one-pass connected pattern with no coffee ring in the channel. Figure 4(b) shows one-pass separate lines printed at low speed (100 μm s^{-1}), which has caused random high and low concentrations of CNTs, while CNTs are not drawn to line borders at the edges, as there is no well-defined coffee ring. Blue arrows point to the line edges in each image. The improved performance of one-pass separate lines printed at higher speed (400 μm s^{-1}) can be explained by the formation of distinguished lines of interwoven CNTs in figure 4(c) where the tubes are connected. Figure 4(d) shows AFM images of two-pass separate lines, which doubles the overall concentration of CNTs compared with one-pass separate line patterns (figure 4(c)) and exhibits wider paths of interwoven CNTs. These images along with results in figure 3 and table 1, demonstrate a direct relationship between the intensity of the coffee ring effect and transistor performance.

Having nanotubes with different diameters means having different regions with different intrinsic mobility. In a nanotube network, different lengths, diameters and chiralities determine the intra-tube transport and they all contribute to the average electronic properties. Moreover, the junctions have a tremendous effect on the carrier transport between the tubes, which manifests itself as

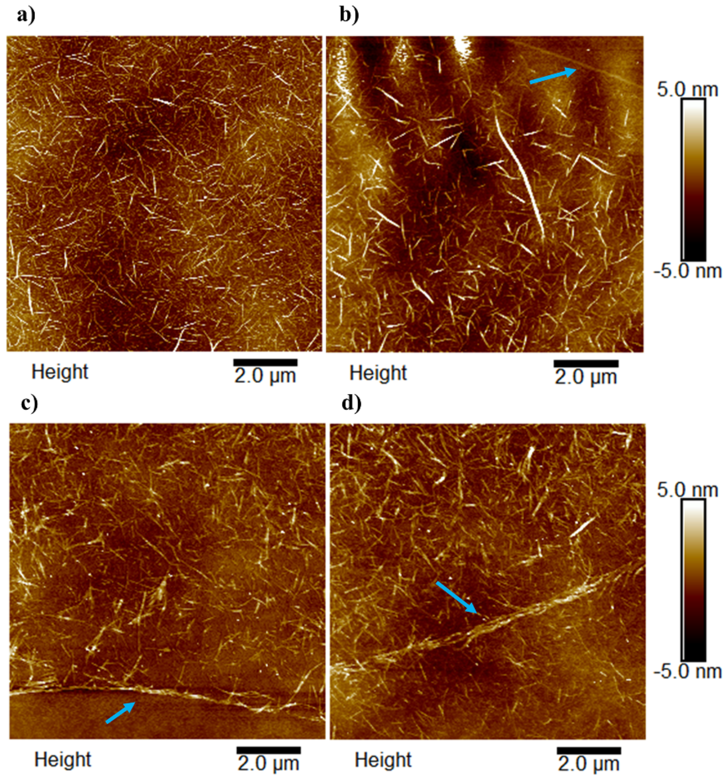

Figure 4. AFM images of printed patterns of (a) one-pass connected lines, (b) one-pass separate lines printed at 100 μm s^{-1}, (c) one-pass separate lines printed at 400 μm s^{-1}, and (d) two-pass separate lines printed at 400 μm s^{-1}. A blue arrow shows the printed line edges in (b)–(d). In (c) and (d), interwoven tubes can be observed on the line edges.

tube-to-tube resistance [53]. Tunneling between two tubes apart from their energy band gaps also depends on the angle of the junction [54]. The angle determines the atomic structure at the junction, and when the tubes are in-registry, the junction resistance is low. Certain junction angles cause the tubes to be in-registry [55]. When coffee ring effect happens, as AFM images demonstrate, the tubes form paths by getting entangled on the edge, in other words, they get knit together forming paths with lower resistance. This can increase the probability of tubes having an in-registry configuration, therefore leading to a decrease in tube-to-tube resistance and eventually the channel resistance. The macroscopic manifestation of this effect is the increase of mobility and decrease of contact resistance measured through I–V characteristics of the device.

It is noteworthy that in the one-pass connected line pattern (random network) the drain current does not saturate at high drain voltages. This behavior is characteristic of random network CNT transistors, mainly due to the presence of metallic tubes [44, 56]. However, the devices with coffee ring induced alignment show an improved level of drain current saturation. In fact, linear output curves at low V_d and drain current saturation at high V_d have been previously reported with spin-aligned CNTs in solution-processed CNT transistors [57]. Here, CNT alignment is achieved in bundles by printing the CNT ink in separate lines with coffee ring. The alignment of tubes along the channel length leads to an effective shortening of the channel as each tube crosses a larger portion of the channel. Furthermore, the formation of CNT bundles decreases the tube-to-tube resistance since there will be a higher probability of tubes having an in-registry configuration where the tube–tube junction angle is low [55]. Therefore, both on-current and off-current increase in the two-pass separate line patterns (figure 3(a)). However, this does not deteriorate drain current saturation (figure 3(c) bottom). The reason is that the alignment of CNTs along the channel increases the percolation threshold [58–61] because it reduces the probability of the tubes, both semiconducting and metallic, connecting with each other (see schematics figure 1, line patterns in second and third rows). Since the concentration of metallic tubes is significantly lower than the concentration of semiconducting tubes (99.9% semiconducting tubes in the ink), this increase in percolation threshold affects metallic tubes more strongly than semiconducting tubes, which leads to an improvement in current saturation, which is deteriorated by metallic tubes in the random network. Therefore, the simultaneous effects of alignment and bundling of the CNTs along the channel lead to a decrease in the resistance while improving drain current saturation in the devices.

The inkjet printing with controlled speed that induces the coffee ring effect not only changes the low-field mobility in the channel, which is independent of contact effects, it also improves the contact resistance. Devices with connected line patterns exhibit a Schottky barrier at the contacts, which is evident from the non-linear output characteristics at low drain current (figure 3(c)), while the aligned patterns are more linear. As was discussed previously to explain the high field effect mobility, the interwoven CNTs have a more in-registry configuration compared to random networks allowing better contact between metal coated CNTs and the channel. Better alignment with the channel also means that more CNTs are in contact with the source and drain electrodes lowering contact resistance. Therefore, their contact with the electrodes becomes more ohmic [57]. This leads to better current injection from the electrodes to the aligned CNTs which is observed as a decrease in contact resistance.

4. Conclusions

With inkjet printing of the CNT transistor channel, the CNT concentration is reduced, but the randomness of their distribution can be manipulated. While ensuring both high mobility and high on–off current ratio with inkjet printing is difficult, separating the printed lines in the pattern and forming a coffee ring results in considerable improvement in all transistor properties. The coffee ring effect, which can be controlled by printing speed and number of layers, regulates the CNT network in the channel. By changing one-pass connected lines to one-pass separate lines and to two-pass separate lines, the field-effect mobility extracted at the drain voltage of -2 V increases from 1.1 to 1.5 to 5.7 cm^2 V^{-1} s^{-1} and the on–off current ratio changes from 2.3×10^5 to 8.2×10^5 to 3.6×10^5. The YFM shows a higher low-field channel mobility and lower contact resistance caused by the coffee ring induced regulated tubes compared with a random CNT network. These results can be explained by the lower tube-to-tube resistance of CNTs in the thicker line edge regions with interwoven CNTs for separate line patterns compared to connected lines. With these capabilities, inkjet printing is a promising technique to form CNT channels in TFTs. Inkjet printing of functional inks offers flexibility over pattern design and control over material distribution. Future work can be done on reducing the droplet volume and varying environmental conditions such as temperature and substrate surface roughness to further control the inkjet printing of the channel. We hypothesize that a similar effect could be achieved on other substrates, but it may require further optimization of the printing parameters and surface functionalization. Understanding and controlling these fluidic, surface-related, and thermodynamic aspects are critical for optimizing inkjet printing processes. Further scientific investigation into the interplay of these factors can lead to enhanced control over the deposition patterns, ultimately improving the uniformity and performance of printed electronic devices.

Data availability statement

All data that support the findings of this study are included within the article (and any supplementary files).

Acknowledgments

We acknowledge the support of the Natural Sciences and Engineering Research Council of Canada (NSERC), funding reference numbers STPGP 521480-18 and ALLRP 578632-22. AFM and optical profilometry images were taken at the Mechanical Engineering department at York University.

Author contributions

The manuscript was written through contributions of all authors. All authors have given approval to the final version of the manuscript.

ORCID iD

Paria Naderi https://orcid.org/0000-0003-4725-6057

References

[1] Khan Y, Thielens A, Muin S, Ting J, Baumbauer C and Arias A C 2020 A new frontier of printed electronics: flexible hybrid electronics *Adv. Mater.* **32** 1905279
[2] Bonnassieux Y *et al* 2021 The 2021 flexible and printed electronics roadmap *Flex. Print. Electron.* **6** 023001
[3] Grau G, Kitsomboonloha R, Swisher S L, Kang H and Subramanian V 2014 Printed transistors on paper: towards smart consumer product packaging *Adv. Funct. Mater.* **24** 5067–74
[4] Cardenas J A, Catenacci M J, Andrews J B, Williams N X, Wiley B J and Franklin A D 2018 In-place printing of carbon nanotube transistors at low temperature *ACS Appl. Nano Mater.* **1** 1863–9
[5] Seifert T, Sowade E, Roscher F, Wiemer M, Gessner T and Baumann R R 2015 Additive manufacturing technologies compared: morphology of deposits of silver ink using inkjet and aerosol jet printing *Ind. Eng. Chem. Res.* **54** 769–79
[6] Singh R S, Takagi K, Aoki T, Moon J H, Neo Y, Iwata F, Mimura H and Moraru D 2022 Precise deposition of carbon nanotube bundles by inkjet-printing on a CMOS-compatible platform *Materials* **15** 4935
[7] Beecher P *et al* 2007 Ink-jet printing of carbon nanotube thin film transistors *J. Appl. Phys.* **102** 043710
[8] Schindler A, Brill J, Fruehauf N, Novak J P and Yaniv Z 2007 Solution-deposited carbon nanotube layers for flexible display applications *Physica* E **37** 119–23
[9] Cai L, Zhang S, Miao J, Yu Z and Wang C 2016 Fully printed stretchable thin-film transistors and integrated logic circuits *ACS Nano* **10** 11459–68
[10] Yu M, Wan H, Cai L, Miao J, Zhang S and Wang C 2018 Fully printed flexible dual-gate carbon nanotube thin-film transistors with tunable ambipolar characteristics for complementary logic circuits *ACS Nano* **12** 11572–8

[11] Kim B, Geier M L, Hersam M C and Dodabalapur A 2015 Inkjet printed circuits on flexible and rigid substrates based on ambipolar carbon nanotubes with high operational stability *ACS Appl. Mater. Interfaces* **7** 27654–60
[12] Chen H, Cao Y, Zhang J and Zhou C 2014 Large-scale complementary macroelectronics using hybrid integration of carbon nanotubes and IGZO thin-film transistors *Nat. Commun.* **5** 4097
[13] Cao X, Wu F, Lau C, Liu Y, Liu Q and Zhou C 2017 Top-contact self-aligned printing for high-performance carbon nanotube thin-film transistors with sub-micron channel length *ACS Nano* **11** 2008–14
[14] Kim B, Geier M L, Hersam M C and Dodabalapur A 2017 Inkjet printed circuits based on ambipolar and P-type carbon nanotube thin-film transistors *Sci. Rep.* **7** 39627
[15] Ervasti H, Järvinen T, Pitkänen O, Bozó É, Hiitola-Keinänen J, Huttunen O H, Hiltunen J and Kordas K 2021 Inkjet-deposited single-wall carbon nanotube micropatterns on stretchable PDMS-Ag substrate-electrode structures for piezoresistive strain sensing *ACS Appl. Mater. Interfaces* **13** 27284–94
[16] Ammu S, Dua V, Agnihotra S R, Surwade S P, Phulgirkar A, Patel S and Manohar S K 2012 Flexible, all-organic chemiresistor for detecting chemically aggressive vapors *J. Am. Chem. Soc.* **134** 4553–6
[17] Beyer S T and Walus K 2012 Controlled orientation and alignment in films of single-walled carbon nanotubes using inkjet printing *Langmuir* **28** 8753–9
[18] Kordás K, Mustonen T, Tóth G, Jantunen H, Lajunen M, Soldano C, Talapatra S, Kar S, Vajtai R and Ajayan P M 2006 Inkjet printing of electrically conductive patterns of carbon nanotubes *Small* **2** 1021–5
[19] Artukovic E, Kaempgen M, Hecht D S, Roth S and Grüner G 2005 Transparent and flexible carbon nanotube transistors *Nano Lett.* **5** 757–60
[20] Bo X Z, Lee C Y, Strano M S, Goldfinger M, Nuckolls C and Blanchet G B 2005 Carbon nanotubes-semiconductor networks for organic electronics: the pickup stick transistor *Appl. Phys. Lett.* **86** 182102
[21] Rozlosnik N, Gerstenberg M C and Larsen N B 2003 Effect of solvents and concentration on the formation of a self-assembled monolayer of octadecylsiloxane on silicon (001) *Langmuir* **19** 1182–8
[22] Okimoto H, Takenobu T, Yanagi K, Miyata Y, Shimotani H, Kataura H and Iwasa Y 2010 Tunable carbon nanotube thin-film transistors produced exclusively via inkjet printing *Adv. Mater.* **22** 3981–6
[23] Oh H, Kim H, Yoo H, Park B, Chung S, Lee B and Hong Y 2021 Inkjet-printing-based density profile engineering of single-walled carbon nanotube networks for conformable high-on/off-performance thin-film transistors *ACS Appl. Mater. Interfaces* **13** 43163–73
[24] Numata H, Ihara K, Saito T, Endoh H and Nihey F 2012 Highly uniform thin-film transistors printed on flexible plastic films with morphology-controlled carbon nanotube network channels *Appl. Phys. Express* **5** 055102
[25] Liu R, Ding H, Lin J, Shen F, Cui Z and Zhang T 2012 Fabrication of platinum-decorated single-walled carbon nanotube based hydrogen sensors by aerosol jet printing *Nanotechnology* **23** 505301
[26] Deegan R D, Bakajin O, Dupont T F, Huber G, Nagel S R and Witten T A 1997 Capillary flow as the cause of ring stains from dried liquid drops *Nature* **389** 827–9
[27] Yunker P J, Still T, Lohr M A and Yodh A G 2011 Suppression of the coffee-ring effect by shape-dependent capillary interactions *Nature* **476** 308–11
[28] Song J W, Kim J, Yoon Y H, Choi B S, Kim J H and Han C S 2008 Inkjet printing of single-walled carbon nanotubes and electrical characterization of the line pattern *Nanotechnology* **19** 095702
[29] Cui L, Zhang J, Zhang X, Li Y, Wang Z, Gao H, Wang T, Zhu S, Yu H and Yang B 2012 Avoiding coffee ring structure based on hydrophobic silicon pillar arrays during single-drop evaporation *Soft Matter* **8** 10448–56
[30] Lim J A, Lee W H, Lee H S, Lee J H, Park Y D and Cho K 2008 Self-organization of ink-jet-printed triisopropylsilylethynyl pentacene via evaporation-induced flows in a drying droplet *Adv. Funct. Mater.* **18** 229–34
[31] Fukuda K, Takeda Y, Kobayashi Y, Shimizu M, Sekine T, Kumaki D, Kurihara M, Sakamoto M and Tokito S 2013 Patterning method for silver nanoparticle electrodes in fully solution-processed organic thin-film transistors using selectively treated hydrophilic and hydrophobic surfaces *Jpn. J. Appl. Phys.* **52** 05DB05
[32] Hu G *et al* 2017 Black phosphorus ink formulation for inkjet printing of optoelectronics and photonics *Nat. Commun.* **8** 1–10
[33] Ko H and Tsukruk V V 2006 Liquid-crystalline processing of highly oriented carbon nanotube arrays for thin-film transistors *Nano Lett.* **6** 1443–8
[34] Liu L *et al* 2020 Aligned, high-density semiconducting carbon nanotube arrays for high-performance electronics *Science* **368** 850–6
[35] Park B, Jang J, Kim H, Seo J, Yoo H, Kim T and Hong Y 2022 Enhanced current path by circularly and periodically-aligned semiconducting single-walled carbon nanotubes for logic circuit device *Flex. Print. Electron.* **7** 015005
[36] Fischer B J 2002 Particle convection in an evaporating colloidal droplet *Langmuir* **18** 60–67
[37] Inanlu M J, Farhadi J, Ansari E, Charkas S and Bazargan V 2022 Effect of surfactant concentration on the evaporation-driven deposition of carbon nanotubes: from coffee-ring effect to strain sensing *RSC Adv.* **12** 31688–98
[38] Zang D, Tarafdar S, Tarasevich Y Y, Dutta Choudhury M and Dutta T 2019 Evaporation of a droplet: from physics to applications *Phys. Rep.* **804** 1–56
[39] Zhang Y, Chen X, Liu F, Li L, Dai J and Liu T 2018 Enhanced coffee-ring effect via substrate roughness in evaporation of colloidal droplets *Adv. Condens. Matter Phys.* **2018** 9795654
[40] Sefiane K 2014 Patterns from drying drops *Adv. Colloid Interface Sci.* **206** 372–81
[41] Hu H and Larson R G 2005 Analysis of the effects of Marangoni stresses on the microflow in an evaporating sessile droplet *Langmuir* **21** 3972–80
[42] Brutin D and Starov V 2018 Recent advances in droplet wetting and evaporation *Chem. Soc. Rev.* **47** 558
[43] Soltman D and Subramanian V 2008 Inkjet-printed line morphologies and temperature control of the coffee ring effect *Langmuir* **24** 2224–31
[44] Cao C, Andrews J B, Kumar A and Franklin A D 2016 Improving contact interfaces in fully printed carbon nanotube thin-film transistors *ACS Nano* **10** 5221–9
[45] Cardenas J A, Upshaw S, Williams N X, Catenacci M J, Wiley B J and Franklin A D 2019 Impact of morphology on printed contact performance in carbon nanotube thin-film transistors *Adv. Funct. Mater.* **29** 1805727
[46] Ravi S, Kaiser A B and Bumby C W 2010 Improved conduction in transparent single walled carbon nanotube networks drop-cast from volatile amine dispersions *Chem. Phys. Lett.* **496** 80–85
[47] Wang C, Wang Y, Yao Y, Luo W, Wan J, Dai J, Hitz E, Fu K and Hu L 2016 A solution-processed high-temperature, flexible, thin-film actuator *Adv. Mater.* **28** 8618–24
[48] Lau P H, Takei K, Wang C, Ju Y, Kim J, Yu Z, Takahashi T, Cho G and Javey A 2013 Fully printed, high performance carbon nanotube thin-film transistors on flexible substrates *Nano Lett.* **13** 3864–9
[49] Street R A and Salleo A 2002 Contact effects in polymer transistors *Appl. Phys. Lett.* **81** 2887
[50] Xu Y, Minari T, Tsukagoshi K, Chroboczek J A and Ghibaudo G 2010 Direct evaluation of low-field mobility and access resistance in pentacene field-effect transistors *J. Appl. Phys.* **107** 114507
[51] Naderi P and Grau G 2022 Organic thin-film transistors with inkjet-printed electrodes on hydrophobic Teflon-AF

gate dielectric with reversible surface properties *Org. Electron.* **108** 106612

[52] Lin D W, Bettinger C J, Ferreira J P, Wang C L and Bao Z 2011 A cell-compatible conductive film from a carbon nanotube network adsorbed on poly-L-lysine *ACS Nano* **5** 10026–32

[53] Schießl S P, De Vries X, Rother M, Massé A, Brohmann M, Bobbert P A and Zaumseil J 2017 Modeling carrier density dependent charge transport in semiconducting carbon nanotube networks *Phys. Rev. Mater.* **1** 46003

[54] Zorn N F and Zaumseil J 2021 Charge transport in semiconducting carbon nanotube networks *Appl. Phys. Rev.* **8** 041318

[55] Klimm W and Kwok K 2022 Tunneling resistance model for piezoresistive carbon nanotube polymer composites *Nanotechnology* **34** 045502

[56] Gong Q, Bhatt V D, Albert E, Abdellah A, Fabel B, Lugli P and Scarpa G 2014 On the performance of solution-processable random network carbon nanotube transistors: unveiling the role of network density and metallic tube content *IEEE Trans. Nanotechnol.* **13** 1181–5

[57] Choi S-J, Wang C, Chi Lo C, Bennett P, Javey A and Bokor J 2012 Comparative study of solution-processed carbon nanotube network transistors *Appl. Phys. Lett.* **101** 112104

[58] Balberg I, Binenbaum N and Anderson C H 1983 Critical behavior of the two-dimensional sticks system *Phys. Rev. Lett.* **51** 1605

[59] Balberg I and Binenbaum N 1983 Computer study of the percolation threshold in a two-dimensional anisotropic system of conducting sticks *Phys. Rev.* B **28** 3799

[60] Munson-Mcgee S H 1991 Estimation of the critical concentration in an anisotropic percolation network *Phys. Rev.* B **43** 3331

[61] Hoffmann T, Martínez-Salazar J, Herrero P and Petermann J 1997 Percolative behavior of an anisotropic two-dimensional network: growth of tellurium onto an oriented polymer film *Phys. Rev.* B **55** 1858